Nanocapsules

DOI: 10.1002/anie.201005662

Drug Delivery Using Nanoparticle-Stabilized Nanocapsules**

*Xiao-Chao Yang, Bappaditya Samanta, Sarit S. Agasti, Youngdo Jeong, Zheng-Jiang Zhu, Subinoy Rana, Oscar R. Miranda, and Vincent M. Rotello**

Microcapsules (MCs) are versatile systems with applications in areas as diverse as microreactors, catalysis,[1] diagnostics, and drug delivery.[2] In these systems, self-assembly of lipids and/or polymers can be used to generate several types of nano- and microcapsules. These include vesicular structures such as liposomes,[3] polymerosomes,[4] colloidosomes,[5] and polyelectrolyte capsules that feature aqueous interiors and exteriors.[6] An alternate motif is provided by emulsions, where additives are used to stabilize the interface between immiscible fluids to produce, for example, oil-in-water emulsions.[7] Through tailoring the composition and structure of the building blocks, MCs of both types can be engineered with well-defined structures, functions, and stability.[8] MCs provide excellent delivery vehicles for biomedical applications, featuring high payload-to-carrier ratios and protection of encapsulated materials from degradation.

Nanoparticle-stabilized capsules (NPSCs) present microcapsule structural motifs where the nanoparticles[9] are assembled at the interface of immiscible solvent droplets. The physical properties of NPSCs can be precisely controlled in a modular fashion through the proper choice of nanoparticle precursors and assembly conditions,[10] giving these systems utility in numerous applications.[11] In NPSCs, nanoparticles in the capsule shell serve as modular building blocks, allowing incorporation of the particle properties into the functional capabilities of the microcapsules. When used as delivery vehicles, these oil-in-water emulsion particles are ideally suited for transport of hydrophobic drugs, making these systems complementary to their vesicular counterparts, for example, liposomes or polymerosomes. The nanoparticle shell of NPSCs imparts additional functional capabilities; for example, nanoparticles can serve as antennae leading to controlled release of materials encapsulated in the microcapsules by responding to external stimuli (e.g. magnetic fields or laser light).[12] Additionally, the inherent rigidity of the particles and the capsule shell offer encapsulation vehicles with mechanical advantage as compared to the soft, self-assembled shell made of polymers or lipids.[13] The permeability of the NPSCs can be tailored through variation of the dimension of the colloidal particles, as shown by Duan and coworkers,[11c] who fabricated magnetic NPSCs with tunable permeability by assembling different sized magnetite (Fe_3O_4) nanoparticles at the interfaces of water-in-oil (W/O) droplets.

Capsule size plays a pivotal role for the applications of MCs in catalysis, nanoreactors,[14] and sensors,[15] with decreasing size generally providing more effective systems. Likewise, carrier size is critical for application in drug delivery processes: carrier size controls the perfusion of materials through the endothelium and the diffusion of materials through tissues. For longer circulation times, the size of the carrier should be small enough (<200 nm) to escape capture and subsequent removal by the resident macrophages in the reticuloendothelial system, such as the liver and spleen.[16] In this respect, materials with diameters between 10 and 200 nm are particularly useful due to their enhanced bioavailability and their ability to take advantage of the enhanced permeation and retention (EPR) effect.[17] For NPSCs to be useful in the delivery context, they will need to have a proper size ($10 \leq d \leq 200$ nm) for optimal activity.

A variety of techniques, for example, tuning of particle wettability[12] or lateral crosslinking[18] of the particles at interface, have been developed to address the stability of nanoparticles on the capsule shells. However, despite progress in this field, current methods generate NPSCs ranging from several micrometers to millimeters. The fabrication of smaller NPSCs encounters two challenges. First, the confinement of particles on droplets surface is driven by total interfacial energy decrease.[19] The three contributions to the interfacial energy arise from the particle–oil interface ($\gamma_{P/O}$), the particle–water interface ($\gamma_{P/W}$), and the oil–water interface ($\gamma_{O/W}$). The effective decrease in interfacial energy due to the assembly of a single particle at the oil–water interface is given by Equation (1), where γ and r are the interfacial tension between two adjacent phases and the effective radius of the particle, respectively.[20]

$$\Delta E = -\frac{\pi r^2}{\gamma_{O/W}}[\gamma_{O/W} - (\gamma_{P/W} - \gamma_{P/O})]^2 \quad (1)$$

Because ΔE depends on r^2, the energy decrease is smaller (and is comparable to the thermal energy) for small particles than for larger ones. Consequently, interfacially confined nanoparticles are more prone towards spatial fluctuations and

[*] Dr. X.-C. Yang, Dr. B. Samanta,[+] S. S. Agasti,[+] Y. Jeong, Z.-J. Zhu, S. Rana, O. R. Miranda, Prof. V. M. Rotello
Department of Chemistry, University of Massachusetts Amherst
710 North Pleasant Street, Amherst, MA 01003 (USA)
Fax: (+1) 413-545-2058
E-mail: rotello@chem.umass.edu
Dr. X.-C. Yang
College of Biomedical Engineering and Medical Imaging
Third Military Medical University, Chongqing, 400030 (China)

[+] These authors contributed equally to this work.

[**] This research was supported by the NIH (GM077173 and EB012246-01) and MRSEC facilities. S.S.A. acknowledges a University of Massachusetts Graduate School Fellowship. X.C.Y. gratefully acknowledges support from the China Scholarship Council for the State Scholarship Fund.

Supporting information for this article is available on the WWW under http://dx.doi.org/10.1002/anie.201005662.

eventual displacement from the interface. A second issue is that stabilization of capsules relies on the Laplace pressure, that is, the pressure difference between the inside and outside of the capsules. This effect is caused by the surface tension of the interface between the solvents[21] and is given as Equation (2), where G is the radius of the capsules.

$$\Delta P = 2\gamma_{o/w}/G \quad (2)$$

It is evident from Equation (2) that as capsule size decreases, the Laplace pressure exerted to the interfacial nanoparticles increases, making smaller droplets unstable. As a result smaller droplets tend to coalesce in solution. Taken together, as capsule size decreases there is less driving force for the nanoparticle to move to the interface, an effect that is exacerbated by the higher surface area of nanometer-scale capsules.

To generate the nanoscale NPSCs required for delivery applications, we have investigated an alternative strategy that relies upon nanoscale droplet stabilization through supramolecular interactions. Two different supramolecular strategies were combined to tune interfacial energy and stabilize the nanoparticle shell of NPSCs (Figure 1). First, we have engineered the interaction between the nanoparticle that constitute the NPSC shell with the "oil" interior of the capsule to access nanoscale assemblies. Second, the NPSC architecture was stabilized through lateral particle–particle interactions. By utilizing this combined approach, we have developed a direct and versatile technique for the creation of NPSCs featuring diameters as small as around 100 nm that are stable in buffer as well as in media and serum.

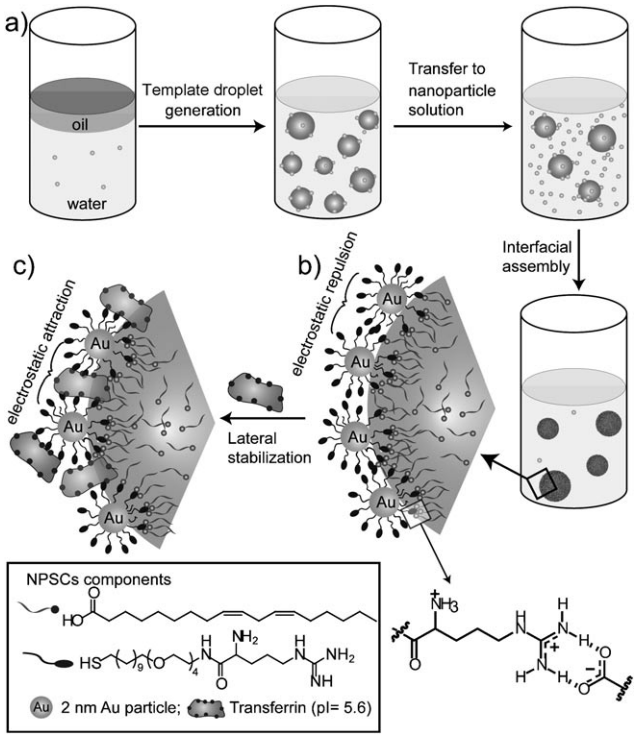

Figure 1. Fabrication of stable nanoscale NPSCs. a) Generation of nanosized oil-in-water droplets followed by interfacial assembly of arginine-functionalized gold nanoparticles. b) Supramolecular interactions between nanoparticle and linoleic acid droplets through arginine–carboxylate interactions. c) Transforming strong particle–particle repulsion to a stabilizing electrostatic attraction by lateral noncovalent cross-linking of particles using transferrin protein.

Our initial efforts to produce stable NPSCs focused on the use of nanoparticle–droplet interactions to stabilize the particle shell. The well-known arginine–carboxylate hydrogen bonding/electrostatic interaction[22] was exploited through use of biocompatible linoleic acid as the "oil", and arginine-functionalized gold nanoparticles (AuNP-Arg, core diameter ca. 2 nm) as the nanoparticle shell. Other than the required surface functionality, gold nanoparticles also provide a biocompatible and nontoxic platform,[23] which is well-suited for delivery applications. The stable nanoscale NPSCs were produced by a three-step procedure. First, template droplets with an approximate size of 105 nm were generated by agitating linoleic acid in phosphate buffer (5 mM, pH 7.4) in the presence of a small amount of AuNP-Arg using a commercial homogenizer. In the second step, the droplets were transferred into solutions of AuNP-Arg. This dispersion process results in essentially instantaneous assembly of the arginine nanoparticles at the droplet surface through arginine–carboxylate hydrogen bonding/electrostatic interactions, generating nanoscale NPSCs. NPSC formation was optimized by varying the nanoparticle/droplet ratio, and the resultant assemblies were characterized by TEM (see Supporting Information Figure S3a–c). The optimized nanoparticle/droplet ratio for successful nanoscale NPSC formation was 2.5 μM/0.64 nM (on a per droplet basis). At this optimum ratio, the TEM image shows essentially no free nanoparticles on the sample grid and a dense packing of nanoparticles on the droplets. The average number of AuNP-Arg nanoparticles bound to a single linoleic acid droplet estimated is 4061 (see Supporting Information for the calculation).

Two analogues of linoleic acid (methyl linolate and linoleoyl alcohol) were used as controls to verify that NPSC formation was driven by guanidinium–carboxylate interactions. As shown in Figure 2a, the arginine nanoparticles bind to linoleic acid droplets, forming NPSCs that could be readily pelleted by centrifugation (at a speed of 3000 rpm, 5 min). Significantly, no free particle was observed after centrifugation, indicating complete incorporation of AuNP-Arg into the NPSC shell. In contrast, no NPSC formation was observed with the controls. The confinement of AuNP-Arg at linoleic acid droplets surface was also evidenced from encapsulating fluorescent Nile Red dye into the oil droplets followed by nanoparticle assembly and centrifugation. As shown in Figure 2b, Nile Red encapsulated droplets showed intensive red fluorescence while no fluorescence signal was detected from the supernatant of NPSCs after centrifugation, indicating effective binding of nanoparticles to the droplets.

Further evidence of the strong interaction between the AuNP-Arg particles and the linoleic acid droplets was obtained using isothermal titration calorimetry (ITC) study, where AuNP-Arg was titrated into a buffered (5 mM phosphate buffer, pH 7.4) suspension of each of the three oil droplets. The ITC results indicated that the interactions between the nanoparticle and oil droplets made from each of

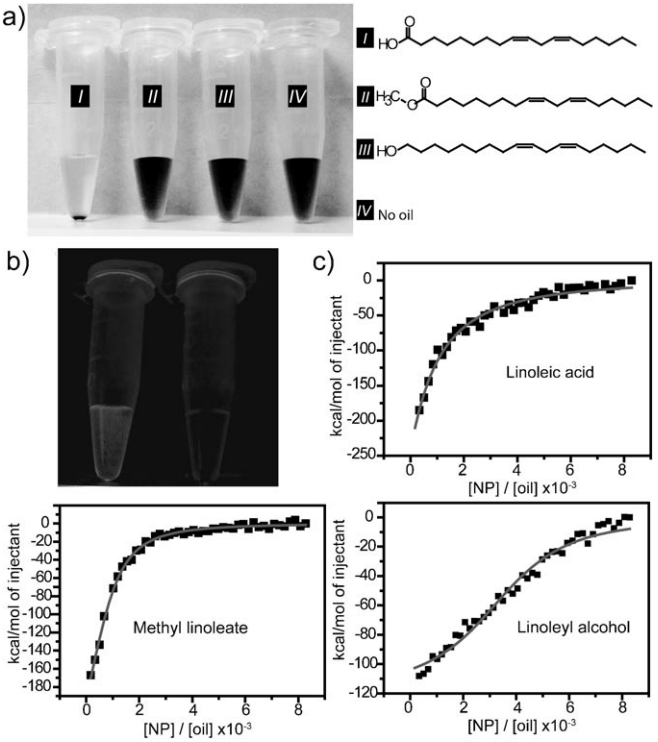

Figure 2. Controlling supramolecular interactions to create NPSCs. a) NPSC formation with linoleic acid whereas no NPSC assembly was observed using controls. b) Photograph of Nile Red encapsulated linoleic acid NPSCs containing vial under UV light before (left) and after (right) centrifugation of NPSCs (see Figure S7 for color image). c) ITC titration of AuNP-Arg nanoparticles into a buffered (5 mM, pH 7.4) suspension of each of the three oil droplets. The squares represent the integrated heat changes during complex formation and the lines represent the curve fit to the binding isotherm.

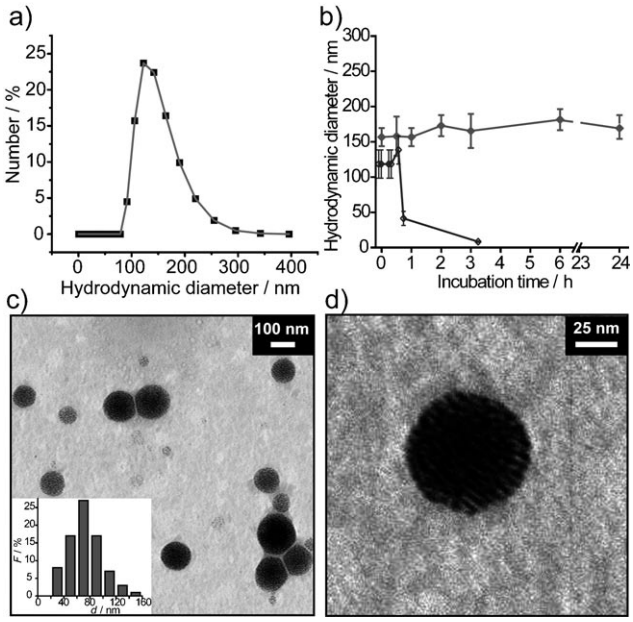

Figure 3. Size and shape of NPSCs in different conditions. a) Hydrodynamic diameter as observed by DLS measurement of protein-stabilized NPSCs in phosphate buffer (5 mM, pH 7.4). NPSCs fabricated by assembly of 0.64 nM droplets with 2.5 μM nanoparticle solution followed by lateral cross-linking of particles using transferrin proteins. b) Stability study of linoleic acid NPSCs with (◆) and without transferrin (◇) in physiological condition over time. c) TEM image of NPSCs. The inset shows the size distribution determined from TEM image by counting the diameter *d* of 80 individual NPSCs. F: frequency. d) Magnified view of a protein-stabilized NPSC.

the three oils were all exothermic in nature. Significantly, the ΔH for linoleic acid (-17.6 kcal mol^{-1}) was far more exothermic than that observed for methyl linoleate (-0.3 kcal mol^{-1}) and linoleyl alcohol (-0.1 kcal mol^{-1}; Figure 2c and Figure S4), indicative of the strong interaction between arginine and linoleic acid.

The AuNP-Arg–linoleic acid capsules assemblies were stable in buffer, however degraded within 3 h in cell culture medium, as observed from the DLS measurement of hydrodynamic diameter (Figure 3b). Our hypothesis was that the low stability of NPSCs under physiological conditions arose from destabilization due to particle–particle repulsion between the highly positively charged AuNP-Arg particles (Figure 1b). In recent studies we have shown that nanoparticles can form stable assemblies with enzymes at oil–water interfaces.[24] Incorporation of complimentary negatively charged transferrin (p$I = 5.6$) proteins into the capsule shell converted the repulsions between AuNP-Arg particles into attractive interactions, generating capsules stable under physiological conditions as demonstrated by DLS (Figure 3b). The dispersity of linoleic acid–transferrin NPSCs was measured by using DLS (Figure 3a). A hydrodynamic diameter of (122 ± 2) nm was observed from this experiment. The protein-stabilized NPSCs were further characterized by using TEM (Figure 3c). The average size distribution (d) determined from TEM image of NPSCs is (75 ± 25) nm. The smaller size observed by TEM is expected, and arises from shrinkage due to drying of the NPSCs in the TEM microscope.

The high stability of the linoleic acid–transferrin NPSCs under physiological conditions makes them potentially useful as delivery vehicles. Preliminary studies of cellular delivery and uptake of NPSCs were performed using a combination of confocal laser scanning microscopy (CLSM) and inductively coupled plasma mass spectrometry (ICP-MS). In these studies, NPSCs loaded with the Nile Red fluorophore were incubated with HeLa cells, and payload delivery followed using CLSM. As shown in Figure 4a,b and Figure S7, efficient delivery of Nile Red to the cytosol was observed after 3 h. There are two potential mechanisms for this payload delivery using these NPSCs. In one mechanism, material is transferred through membrane fusion from the NPSC to the cell without NPSC uptake. In the second mechanism, the cell takes up the intact particle through an endocytotic mechanism, with payload release occurring inside the cell. To differentiate between these mechanisms, we performed a time point analysis. Analysis of cell fluorescence as determined using fluorescence microscopy indicated that maximal uptake was observed after 3 h, with little further increase in fluorescence observed after 6 h (Figure S6a). However, very different kinetics were observed for AuNP-Arg uptake using ICP-MS, in which steadily increasing amounts of intracellular Au were

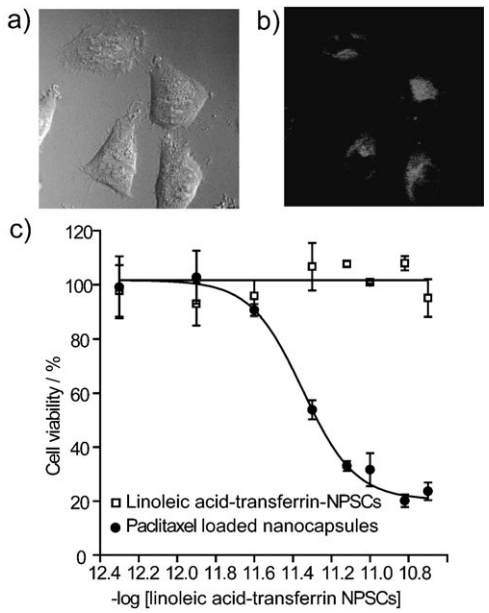

Figure 4. Delivery of Nile Red encapsulated linoleic acid–transferrin NPSCs in HeLa cells. a,b) CLSM images of HeLa cells treated with same NPSCs for 3 h; a) bright field, b) red channel (see Figure S8 for color image). c) Cytotoxicity of paclitaxel-loaded linoleic acid–transferrin NPSCs. The cell viabilities were measured by Alamar blue assay after 24 h incubation of paclitaxel-loaded linoleic acid–transferrin NPSCs and carrier with HeLa cells.

observed over 6 h (Figure S6b). This observation was consistent with the NPSC-cell fusion mechanism. Further support for a non-endocytotic delivery process comes from fluorophore delivery studies using sodium azide and deoxyribose, well known inhibitors of energy-dependent endocytosis through disruption of cellular ATP production. Time point analysis revealed no significant difference in particle uptake (Figure S8) in the presence of either inhibitor, consistent with fluorophore uptake through a non-endocytotic pathway.

Having established effective fluorophore delivery, we next investigated the efficacy of these NPSCs as drug delivery systems in cell culture models. Using the Alamar blue viability assay and HeLa cells, we determined that the linoleic acid–transferrin NPSCs featured no non-specific cytotoxicity at the concentrations studied (Figure 4c). Our initial drug candidate for NPSC-mediated delivery was paclitaxel due to its high toxicity and hydrophobicity. Paclitaxel is one of the most effective anticancer drugs for the treatment of a wide variety of cancers, however this highly hydrophobic drug suffers from poor solubility with concomitant issues in biodistribution.[25] We have used linoleic acid–transferrin NPSCs for paclitaxel encapsulation and delivery purposes due to its high stability under physiological conditions and efficient fluorophore delivery efficiency. Paclitaxel has a relatively high solubility in linoleic acid (10 mg mL^{-1}), allowing high loading of the NPSCs without substantial processing. Delivery studies indicate that release of paclitaxel from the NPSC is quite efficient, with an IC_{50} value for the encapsulated drug of 13.5 ng mL^{-1} (Figure 4c), as compared to 6.5 ng mL^{-1} for free paclitaxel.

In summary, we have developed a strategy for NPSCs fabrication that combines radial particle–lipid and lateral particle–protein supramolecular interactions to generate capsules of unprecedentedly small size (ca. 100 nm). We envision that further modulation of these interactions through the use of diverse chemical functionality will provide a control over the capsule size and functionality for many applications. Cell culture studies of drug delivery into cancer cells using these NPSC carriers demonstrated highly efficient payload delivery with no measurable carrier toxicity. The nanoparticle shell of NPSC provides a platform for future incorporating of targeting molecules to realize targeted cancer therapy for animal studies, a prospect that is currently under investigation.

Received: September 9, 2010
Published online: December 10, 2010

Keywords: drug delivery · gold nanoparticles · interfacial energy · nanocapsules · supramolecular interactions

[1] K. T. Kim, J. J. L. M. Cornelissen, R. J. M. Nolte, J. C. M. van Hest, *Adv. Mater.* **2009**, *21*, 2787 – 2791.
[2] a) Y. Zhao, L. Jiang, *Adv. Mater.* **2009**, *21*, 3621 – 3638; b) R. V. Parthasarathy, C. R. Martin, *Nature* **1994**, *369*, 298 – 301; c) B. G. De Geest, S. De Koker, G. B. Sukhorukov, O. Kreft, W. J. Parak, A. G. Skirtach, J. Demeester, S. C. De Smedt, W. E. Hennink, *Soft Matter* **2009**, *5*, 282 – 291.
[3] V. F. Torchilin, *Nat. Rev. Drug Discovery* **2005**, *4*, 145 – 160.
[4] a) Z. Cheng, D. L. J. Thorek, A. Tsourkas, *Adv. Funct. Mater.* **2009**, *19*, 3753 – 3759; b) J. R. Howse, R. A. L. Jones, G. Battaglia, R. E. Ducker, G. J. Leggett, A. J. Ryan, *Nat. Mater.* **2009**, *8*, 507 – 511.
[5] A. D. Dinsmore, M. F. Hsu, M. G. Nikolaides, M. Marquez, A. R. Bausch, D. A. Weitz, *Science* **2002**, *298*, 1006 – 1009.
[6] a) C. S. Peyratout, L. Dähne, *Angew. Chem. Int. Ed.* **2004**, *116*, 3850 – 3872; *Angew. Chem. Int. Ed.* **2004**, *43*, 3762 – 3783; b) A. N. Zelikin, Q. Li, F. Caruso, *Angew. Chem.* **2006**, *118*, 7907 – 7909; *Angew. Chem. Int. Ed.* **2006**, *45*, 7743 – 7745.
[7] A. B. Subramaniam, M. Abkarian, H. A. Stone, *Nat. Mater.* **2005**, *4*, 553 – 556.
[8] a) B. Wang, L. F. Zhang, S. C. Bae, S. Granick, *Proc. Natl. Acad. Sci. USA* **2008**, *105*, 18171 – 18175; b) L. F. Zhang, K. Dammann, S. C. Bae, S. Granick, *Soft Matter* **2007**, *3*, 551 – 553.
[9] E. Glogowski, R. Tangirala, J. He, T. P. Russell, T. Emrick, *Nano Lett.* **2007**, *7*, 389 – 393.
[10] a) D. Lee, D. A. Weitz, *Adv. Mater.* **2008**, *20*, 3498 – 3503; b) D. Wang, H. Duan, H. Möhwald, *Soft Matter* **2005**, *1*, 412 – 416.
[11] a) B. Binks, R. Murakami, *Nat. Mater.* **2006**, *5*, 865 – 869; b) Z. Nie, A. Petukhova, E. Kumacheva, *Nat. Nanotechnol.* **2010**, *5*, 15 – 25; c) H. Duan, H. D. Wang, N. S. Sobal, M. Giersig, D. G. Kurth, H. Möhwald, *Nano Lett.* **2005**, *5*, 949 – 952.
[12] a) A. G. Skirtach, A. M. Javier, O. Kreft, K. Köhler, A. P. Alberola, H. Möhwald, W. J. Parak, G. B. Sukhorukov, *Angew. Chem.* **2006**, *118*, 4728 – 4733; *Angew. Chem. Int. Ed.* **2006**, *45*, 4612 – 4617; b) S. H. Hu, D. M. Liu, W. L. Tung, C. F. Liao, S. Y. Chen, *Adv. Funct. Mater.* **2008**, *18*, 2946 – 2955.
[13] K. E. Mueggenburg, X. M. Lin, R. H. Goldsmith, H. M. Jaeger, *Nat. Mater.* **2007**, *6*, 656 – 660.
[14] a) D. M. Vriezema, M. C. Aragones, J. A. A. W. Elemans, J. J. L. M. Cornelissen, A. E. Rowan, R. J. M. Nolte, *Chem. Rev.* **2005**, *105*, 1445 – 1490; b) D. M. Vriezema, P. M. L. Garcia, N. Sancho Oltra, N. S. Hatzakis, S. M. Kuiper, R. J. M. Nolte,

A. E. Rowan, J. C. M. van Hest, *Angew. Chem.* **2007**, *119*, 7522 – 7526; *Angew. Chem. Int. Ed.* **2007**, *46*, 7378 – 7382.
[15] X. Zhang, S. Rehm, M. M. Safont-Sempere, F. Würthner, *Nat. Chem.* **2009**, *1*, 623 – 629.
[16] S. M. Moghimi, A. C. Hunter, J. C. Murray, *Pharmacol. Rev.* **2001**, *53*, 283 – 318.
[17] a) I. Brigger, C. Dubernet, P. Couvreur, *Adv. Drug Delivery Rev.* **2002**, *54*, 631 – 651; b) J. A. MacKay, M. Chen, J. R. McDaniel, W. Liu, A. J. Simnick, A. Chilkoti, *Nat. Mater.* **2009**, *8*, 993 – 999; c) S. Sengupta, D. Eavarone, I. Capila, G. Zhao, N. Watson, T. Kiziltepe, R. Sasisekharan, *Nature* **2005**, *436*, 568 – 572; d) E. P. Holowka, V. Z. Sun, D. T. Kamei, T. J. Deming, *Nat. Mater.* **2007**, *6*, 52 – 57.
[18] a) B. Samanta, D. Patra, C. Subramani, Y. Ofir, G. Yesilbag, A. Sanyal, V. M. Rotello, *Small* **2009**, *5*, 685 – 688; b) H. Skaff, Y. Lin, R. Tangirala, K. Breitenkamp, A. Böker, T. P. Russell, T. Emrick, *Adv. Mater.* **2005**, *17*, 2082 – 2086.
[19] P. Pieranski, *Phys. Rev. Lett.* **1980**, *45*, 569 – 572.
[20] Y. Lin, H. Skaff, T. Emrick, A. D. Dinsmore, T. P. Russell, *Science* **2003**, *299*, 226 – 229.
[21] a) D. Myers, *Surfaces, Interfaces, and Colloids—Principles and Applications*, 2nd ed., Wiley-VCH, New York, **1999**; b) T. G. Mason, J. N. Wilking, K. Meleson, C. B. Chang, S. M. Graves, *J. Phys. Condens. Matter* **2006**, *18*, R635 – R666.
[22] a) A. T. Wright, M. J. Griffin, Z. L. Zhong, S. C. McCleskey, E. V. Anslyn, J. T. McDevitt, *Angew. Chem.* **2005**, *117*, 6533 – 6536; *Angew. Chem. Int. Ed.* **2005**, *44*, 6375 – 6378; b) A. Buryak, K. Severin, *J. Am. Chem. Soc.* **2005**, *127*, 3700 – 3701; c) N. Metanis, E. Keinan, P. E. A. Dawson, *J. Am. Chem. Soc.* **2005**, *127*, 5862 – 5868.
[23] E. E. Connor, J. Mwamuka, A. Gole, C. J. Murphy, M. D. Wyatt, *Small* **2005**, *1*, 325 – 327.
[24] B. Samanta, X. C. Yang, Y. Ofir, M. H. Park, D. Patra, S. S. Agasti, O. R. Miranda, Z. H. Mo, V. M. Rotello, *Angew. Chem.* **2009**, *121*, 5445 – 5448; *Angew. Chem. Int. Ed.* **2009**, *48*, 5341 – 5344.
[25] a) E. K. Rowinsky, R. C. Donehower, *N. Engl. J. Med.* **1995**, *332*, 1004 – 1014; b) K. C. Nicolaou, W. M. Dai, R. K. Guy, *Angew. Chem.* **1994**, *106*, 38 – 69; *ngew. Chem. Int. Ed.* **1994**, *33*, 15 – 44.

